Journal of Pathology
J Pathol 2019; **248:** 41–50
Published online 15 February 2019 in Wiley Online Library (wileyonlinelibrary.com) DOI: 10.1002/path.5219

ORIGINAL PAPER

Genomic landscape and evolutionary trajectories of ovarian cancer precursor lesions

Ren-Chin Wu[1†], Pei Wang[2†], Shiou-Fu Lin[3,4†], Ming Zhang[5†], Qianqian Song[2], Tiffany Chu[3], Brant G Wang[6], Robert J Kurman[3], Russell Vang[3], Kenneth Kinzler[5], Cristian Tomasetti[5*], Yuchen Jiao[2*], Ie-Ming Shih[3,5*] and Tian-Li Wang[3,5*]

[1] *Department of Pathology, Chang Gung Memorial Hospital and Chang Gung University School of Medicine, Taoyuan, Taiwan*
[2] *State Key Lab of Molecular Oncology, Laboratory of Cell and Molecular Biology, National Cancer Center/ National Clinical Research Center for Cancer/ Cancer Hospital, Chinese Academy of Medical Sciences and Peking Union Medical College, Beijing, PR China*
[3] *Departments of Pathology and Gynecology/Obstetrics, Johns Hopkins Medical Institutions, Baltimore, MD, USA*
[4] *Department of Pathology, Shuang Ho Hospital, Taipei Medical University, Taipei, Taiwan*
[5] *Department of Oncology, Sidney Kimmel Comprehensive Cancer Center, Johns Hopkins Medical Institutions, Baltimore, MD, USA*
[6] *Department of Pathology, Inova Fairfax Hospital, Falls Church, VA, USA*

**Correspondence to: C Tomasetti, 550 North Broadway, Baltimore, MD 21205, USA. E-mail: ctomasetti@jhu.edu; or Y Jiao, Panjiayuan nanli 17, Chaoyang District, Beijing, PR China 100021. E-mail: jiaoyuchen@126.com; or IM Shih, CRBII, Room 305, 1550 Orleans Street, Baltimore, MD 21231, USA. E-mail: ishih@jhmi.edu; or TL Wang, CRBII, Room 306, 1550 Orleans Street, Baltimore, MD 21231, USA. E-mail: tlw@jhmi.edu*

[†]Authors contributed equally.

Abstract

The clonal relationship between ovarian high-grade serous carcinoma (HGSC) and its presumed precursor lesion, serous tubal intraepithelial carcinoma (STIC), has been reported. However, when analyzing patients with concurrent ovarian carcinoma and tubal lesion, the extensive carcinoma tissues present at diagnosis may have effaced the natural habitat of precursor clone(s), obscuring tumor clonal evolutionary history, or may have disseminated to anatomically adjacent fimbriae ends, masquerading as precursor lesions. To circumvent these limitations, we analyzed the genomic landscape of incidental tubal precursor lesions including p53 signature, dormant STIC or serous tubal intraepithelial lesion (STIL) and proliferative STIC in women without ovarian carcinoma or any cancer diagnosis using whole-exome sequencing and amplicon sequencing. In three of the four cancer-free women with multiple discrete tubal lesions we observed non-identical *TP53* mutations between precursor lesions from the same individual. In one of the four women with co-existing ovarian HGSC and tubal precursor lesion we found non-identical *TP53* mutations and a lack of common mutations shared between her precursor lesion and carcinoma. Analyzing the evolutionary history of multiple tubal lesions in the same four patients with concurrent ovarian carcinoma indicated distinct evolution trajectories. Collectively, the results support diverse clonal origins of tubal precursor lesions at the very early stages of tumorigenesis. Mathematical modeling based on lesion-specific proliferation rates indicated that p53 signature and dormant STIC may take a prolonged time (two decades or more) to develop into STIC, whereas STIC may progress to carcinoma in a much shorter time (6 years). The above findings may have implications for future research aimed at prevention and early detection of ovarian cancer.

Keywords: p53 signatures; STIL; STIC; ovarian cancer; prevention; detection

Received 24 April 2018; Revised 2 December 2018; Accepted 12 December 2018

No conflicts of interest were declared.

Introduction

The early molecular events of ovarian carcinogenesis remain poorly understood, resulting in a lack of effective prevention and early detection strategies [1,2]. Unlike cancers arising in organs such as the colon, where the early events of carcinogenesis can be studied because their precursor lesions are well-recognized, the precursors of ovarian high-grade serous carcinoma (HGSC), the most common and lethal type of ovarian cancer, have eluded detection until recently. Accumulating evidence supports that serous tubal intraepithelial carcinoma (STIC) or its precursor lesions including p53 signature and serous tubal intraepithelial lesion (STIL) located at Fallopian tubes or cortical inclusion cysts of the ovary are the precursors of ovarian HGSC [3–11]. The reported incidence of tubal lesions varied in the literature but when a rigorous sampling was performed in a large cohort of Fallopian tubes from a high-risk population, the incidence of p53 signature and STIC/STIL can be as high as 27 and 12%, respectively [12].

Microscopically, STICs exhibit significant nuclear atypia and architectural alterations, *TP53* mutations and high proliferative/apoptotic activity. STIC cells are

often loosely arranged and can readily disseminate outside the Fallopian tube. The p53 signature is identified as a stretch of 12–30 normal-appearing epithelial cells having a p53 immunoreactivity pattern compatible with a missense *TP53* mutation and displaying low proliferative activity, similar to adjacent normal tubal epithelium. The term STIL has been used to describe, among other lesions, a group of tubal precursors characterized by lower levels of nuclear atypia than STIC, p53 staining patterns compatible with either missense or deleterious TP53 mutations and a level of proliferative activity similar to adjacent normal epithelium [13,14]. 'Dormant STICs' in this study were deemed morphologically compatible with STILs by a panel of gynecological pathologists. Although molecular relationships between STICs and concurrent ovarian HGSCs have been reported [6,15–19], few of these studies analyzed p53 signatures or STILs, largely because of technical challenges. More importantly, as all of these studies analyzed patients with tubal lesions co-existing with advanced ovarian HGSCs, it is likely that some of these lesions were disseminated tumor cell clones from the adjacent, concurrent ovarian tumors, therefore obscuring the evolutionary histories. This issue is aggravated in ovarian HGSCs, which are often diagnosed late, at which time the vast late-stage tumor mass overwhelms or effaces the precursor lesions located at either the Fallopian tube or the small cortical inclusion cysts of the ovary, leaving little trace of the molecular landscape existing before the advent of invasive cancer. Indeed, a recent article cautioned against clonal evolution studies performed on advanced tumors with high genetic heterogeneity and the possibility of constituent clones arising from multiple cell lineages [20]. Consequently, it is difficult to distinguish between true precursor lesions and HGSC implants [15,18]. Nevertheless, powerful techniques for the analysis of clonal evolution are useful for assessing clonal relationships between primary tumor and distant metastases [16,21] and when true precursor lesions are available, the same tools can provide similarly powerful means to delineate tumor evolution.

Here, we aimed to elucidate the genomic landscape of tubal precursor lesions prior to the onset of overt cancer as a means to understand the molecular genetic events occurring at the very early stages of tumorigenesis. We performed whole-exome sequencing on 12 incidental tubal precursor lesions from seven women without a diagnosis of cancer and on an additional six tubal precursor lesions from four patients who had concurrent ovarian HGSCs. We also performed complementary amplicon sequencing on eight incidental tubal precursor lesions from four additional women without concurrent cancer. To our surprise, we observed polyclonal parallel evolution of precursor lesions in some of the women who had multiple lesions. Although a larger study is warranted to determine the clinical significance of molecular genetic events observed in tubal precursor lesions, at the moment our results provide a first glimpse of very early stage, polyclonal features in tumor development, and suggest that not all tubal lesions will progress to carcinoma. We anticipate that these findings will stimulate future research efforts focusing on understanding precancerous lesions and will set the stage for effective prevention and early detection of ovarian cancer.

Materials and methods

Sample collection

All tissue samples (from both in-house and consult collections) were retrieved from the Johns Hopkins Hospital under institutional review board approval (approval no. IRB00127046). Samples had been formalin-fixed and paraffin-embedded (FFPE) and obtained between 2011 and 2017. The inclusion criteria were tubal precursor lesions including p53 signature, STIL and STIC, from women with or without ovarian HGSC. When the lesions were consultation cases we did not record the parity or contraceptive use in the dataset. Furthermore, informed consent could not be obtained, precluding the access to HIPAA (Health Insurance Portability and Accountability Act of 1996, USA)-protected information. The diagnoses of p53 signatures and STICs were based on morphological features and immunohistochemical staining, following the methods described previously [13,14]. p53 signatures were characterized by a background level of proliferative index without cytological atypia, but with nuclear p53 accumulation in 12 or more consecutive secretory cells. Dormant STICs in the current study were morphologically compatible with STILs, characterized by cytological atypia and low proliferative activity (Ki-67 labeling index <10%). In addition, all dormant STICs in this study showed diffuse p53 staining with moderate to strong intensity in more than 75% of cytologically atypical cells, a pattern suggestive of TP53 missense mutations [22]. STICs were composed of secretory cells showing high proliferative index (Ki-67 labeling index ≥10%), with significant atypia and architectural alterations and a mutant p53 staining pattern. All cases were carefully reviewed by at least three pathologists (SFL, RJK, RV, BGW or IMS). Examples of tubal precursor lesions are shown in supplementary material, Figure S1. We analyzed 11 cases that did not have concurrent ovarian HGSCs at the time of diagnosis and four cases that included concurrent ovarian HGSCs and tubal lesions.

Laser capture microdissection (LCM)

Tissue samples were cut in consecutive sequences of 10 serial sections (10 μm thick) for LCM and three additional sections for H&E, p53 and Ki-67 immunostaining to ensure that the target lesions were present in the microdissected sections. LCM was performed immediately after sectioning. Cellular purity was estimated according to the proportion of epithelial cells in the lesion among the total dissected epithelial cells. Epithelial cells from the p53 signature were microdissected using the adjacent slide prestained with p53 as a guide for the dissection.

Whole-exome sequencing and mutation calling analysis

Genomic DNA was extracted from FFPE tissue, including tubal lesions and normal epithelium, after LCM (Leica LMD7000, Buffalo Grove, IL, USA) using the QIAamp FFPE DNA tissue kit (Qiagen, Hilden, Germany). The amount of DNA extracted ranged from ~10 to 120 ng. DNA from four cases of invasive ovarian carcinomas were also prepared. DNA samples were sheared into 150 bp fragments using the M220 focused ultrasonicator (Covaris, Woburn, MA, USA) shearing instrument.

Paired-end libraries were generated from all samples using standard Illumina (San Diego, CA, USA) procedures. Coding regions were captured with the Agilent SureSelect Human All Exon 50 Mb Kit 5.0 (Agilent, Santa Clara, CA, USA) and sequenced on Illumina X10 sequencers with 150PE. Whole-exome sequencing data of matched lesion/tumor and normal samples were aligned to the human reference genome (hg38) using BWA software and analyzed to identify somatic point mutations and small insertions and deletions present in lesion/tumor but not matched normal samples. Single nucleotide variants (SNVs) were detected using MuTect v1 (https://github.com/broadinstitute/mutect) with the following criteria: (1) the mutation was identified in four or more distinct pairs of reads; (2) the number of distinct reads containing a particular mismatched base represented at least 10% of the total number of distinct reads; and (3) the mutation was not present in more than 0.2% of the reads in the matched normal sample. Indels were detected using VarScan v2.3.6. We selected all candidate mutations for visual inspection (Integrative Genomics Viewer; IGV, https://software.broadinstitute.org/software/igv/home).

The functional consequence of each mutation was predicted using gene annotations with ANNOVAR 2018Apr16, using databases from SIFT, Polyphen 2 HDIV prediction and MutationTaster prediction [23]. Cancer-driver genes were defined using guidelines and prediction algorithms, as previously published [24].

Under the stringent calling criteria it was possible that some mutations with lower allele frequency may have been missed, resulting in trunk mutations not identified in all tumor samples. To identify false-negative events, for each somatic mutation called in a sample we examined all other samples from the same patient to determine whether such a mutation actually existed but failed to be detected. A somatic mutation was 'recovered' if it was supported by at least three distinct reads of high quality (minimum base quality score ≥30, minimum mapping quality score ≥20) and had an allele frequency greater than 3%.

Phylogenetic analysis

Both somatic mutations (SNVs and indels) and loss of heterozygosity (LOH) were converted to binary characters to track evolutionary trajectory. We applied the Dollo parsimony method and the branch-and-bound algorithm to find the most parsimonious tree using the Dolpenny program in the package PHYLIP version 3.695 [25]. All phylogenetic trees were rooted at the germline DNA sequence, which was considered the ancestral state with all binary characters set to 0. Phylograms were plotted so that the branch lengths were proportional to the number of somatic mutations and LOH acquired.

Estimating evolutionary time of lesions

Phylogenetic trees were obtained by maximum parsimony. We modeled the numbers of mutations that accumulated by time t in the cell lineage of the Fallopian tube epithelial tissue as an inhomogeneous Poisson process, with its lambda (λ) parameter depending on the stage of the lesion. Ki-67-positive labeling indicated no difference in proliferation rates between cells in normal epithelium and cells in lesions with the p53 signature (see Table 1 and reference [20]). The Ki-67-positive labeling index in normal tissue can be assumed to be exponentially distributed with mean 0.02 (see reference [21]). We therefore used the number of mutations found in each of the three available p53 signature lesions to estimate the λ parameter of the Poisson process via maximum likelihood estimation (MLE) and derived $\lambda = 0.39$. Thus, in normal Fallopian tube epithelium, the exome of each cell accumulates 0.39 mutations per year (or ~39 mutations/year across the entire genome). We also assumed that menarche occurs at 12 years of age [26] and subtracted 12 years from the age of each patient at the time of diagnosis to obtain the numbers of years the tissue underwent active proliferation (post-menarche age). Lesion-specific Ki-67-positive labeling estimates were used to derive lesion-specific λ parameter. The method is described in detail in supplementary material, Supplementary material and methods.

Results

Whole-exome sequencing was performed on the genomic DNA of 18 tubal precursor lesions, from which epithelial cells were carefully isolated by LCM (Figure 1A). These included 12 tubal precursor lesions (three p53 signatures, eight STICs and one dormant STIC) from seven women without an ovarian cancer diagnosis and included six tubal lesions (one p53 signature, two dormant STICs and three STICs) from four women with concurrent ovarian HGSCs. For comparison, we also performed whole-exome sequencing on ovarian HGSCs from these four patients (Table 1 and Figure 1B). None of the women in this cohort carried pathogenic germline *BRCA* mutations (see supplementary material, Table S1). The average distinct exome coverage was 139× (range 63× to 271×) for lesions and 110× (range 85× to 149×) for normal tissues (see supplementary material, Table S2). Within this study cohort we identified 1435 somatic mutations, 1261 of which were confirmed manually by visual inspection with

Table 1. Somatic mutation analysis, proliferation index and estimated evolution time in all lesions studied

Case	Lesion type	Concurrent ovarian cancer	Ki-67 (%)	Number of mutations			Number of LOH	LOH of tumor suppressor genes	TP53 mutation (MAF)	Mutated cancer-driver gene(s)	Evolution times (years from menarche) (±SE)	Years since final lesion (CI:±1SE)
				NS	S	Total						
147	STIC	No	38	38	9	47	7	BRCA1 TP53	H82fs (0.79)	TP53	38	NA
144	STIC	No	20	30	8	38	3	BRCA1 TP53	splice (0.62)	TP53	46	NA
145	STIC	No	12	18	3	21	0		P146S (0.18)	TP53 SOX9	59	7.1 (0–18.7)
11	STIC	No	12	16	4	20	0		R43H (0.23)	TP53 AXIN1	52	NA
59	STIC	No	20	28	7	35	3	BRCA1 TP53	L62P (0.86)	TP53	67	NA
13	B2-STIC	No	20	29	5	34	14	BRCA1 BRCA2 RB1 TP53	H47Q (0.75)	TP53 CIC	44	NA
	B3-STIC	No	19	14	9	23	13	BRCA1 BRCA2 RB1 TP53	Y88X (0.91)	TP53	44	NA
	C1-p53 signature	No	1	8	2	10	0		R150W (0.31)	TP53	44	18.0 (9.8–26.2)
	C3-dormant STIC*	No	3	9	3	12	0		A29D (0.25)	TP53	44	12.8 (3.8–21.8)
	D1-p53 signature	No	1	15	1	16	0		R141H (0.46)	TP53	44	2.4 (0–12.8)
	D2-p53 signature	No	0	9	4	13	0		E226V (0.13)	TP53	44	10.2 (0.8–19.6)
138	STIC	No	12	12	3	15	4	BRCA1 BRCA2 RB1 TP53	E126Q (0.45)	TP53	35	NA
5	A1-HGSC	Yes	20	36	19	55	13	BRCA1 RB1 TP53	L120 fs (0.88)	TP53	60	NA
	D1-p53 signature	Yes	1	23	7	30	2	BRCA1 BRCA2 RB1 TP53	Y88C (0.50)	TP53	60	NA
6	A1-HGSC	Yes	35	41	10	51	18		Y88C (0.57)	TP53 KMT2C	52.7 + 1.3 (±0.4)	NA
	B1-STIC	Yes	35	40	12	52	18		Y88C (0.77)	TP53 KMT2C	52.7 + 1.3 (±0.4)	NA
9	A1-HGSC	Yes	40	101	31	132	19	BRCA1 TP53	R141H (0.95)	TP53	32.7 + 11.3 (±2.2)	NA
	B1-STIC	Yes	30	76	19	95	10	BRCA1 TP53	R141H (0.56)	TP53 NSD1	32.7 + 6.1 (±1.3) + 5.2 (±0.9)	NA
	C1-dormant STIC*	Yes	8	71	16	87	8	BRCA1 TP53	R141H (0.43)	TP53	32.7 + 6.1 (±1.3) + 5.2 (±0.9)	NA
146	A2-HGSC	Yes	20	155	38	193	17	BRCA1 BRCA2 RB1 TP53	C145F (0.97)	TP53 AXIN1 NF2 ATRX	22.9 + 34.1 (±3.1) + 6.0 (±1.2)	NA
	B1-STIC	Yes	15	181	45	226	18	BRCA1 BRCA2 RB1 TP53	C145F (0.89)	TP53 AXIN1 NF2 ATRX	22.9 + 34.1 (±3.1) + 6.0 (±1.2)	NA
	C1-dormant STIC*	Yes	5	44	12	56	0		C145F (0.16)	TP53 NF2	22.9 + 40.1 (±4.3)	32.3 (27.8–36.8)
12	B1-STIC	No	25	N/A	N/A	N/A	N/A	N/A	R175H (0.14)	At least TP53	N/A	N/A
	B2-STIC	No	20	N/A	N/A	N/A	N/A	N/A	G266R (0.14)	At least TP53	N/A	N/A
15	B1-STIC	No	10	N/A	N/A	N/A	N/A	N/A	C141* (0.53)	At least TP53	N/A	N/A
	B2-STIC	No	5	N/A	N/A	N/A	N/A	N/A	L132E (0.37)	At least TP53	N/A	N/A
16	Dormant STIC *	No	4	N/A	N/A	N/A	N/A	N/A	N239S (0.24)	At least TP53	N/A	N/A
111	B1-STIC	No	10	N/A	N/A	N/A	N/A	N/A	C275F (0.10)	At least TP53	N/A	N/A
	C1-dormant STIC*	No	3	N/A	N/A	N/A	N/A	N/A	C275F (0.29)	At least TP53	N/A	N/A
	D1-p53 signature	No	2	N/A	N/A	N/A	N/A	N/A	Y163N (0.05)	At least TP53	N/A	N/A

N/A, not available because whole-exome sequencing was not performed in these small lesions; NS, non-synonymous mutations; MAF, mutant allele frequency; S, synonymous mutations.
*'Dormant STICs' were classified as 'STILs' by gynecological pathologists in this study and should be considered as a subset of STILs according to the classification algorithm published in Vang *et al* [13].

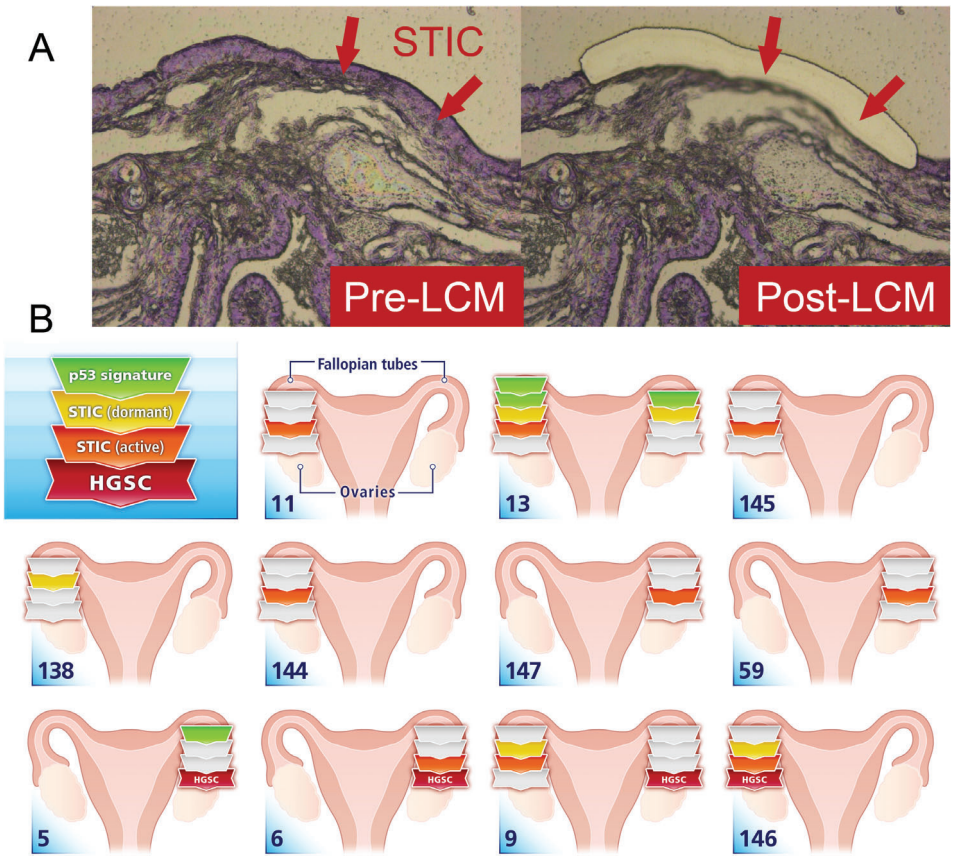

Figure 1. Locations of precursors and cancerous lesions and numbers of somatic mutations detected in these lesions. (A) Representative tissue section containing STIC before and after LCM. Arrows indicate the locations of STICs before (left) and after (right) LCM. (B) Schematic of lesion distribution in 11 patients whose lesions were analyzed by whole-exome sequencing. Red bars, HGSCs; orange bars, proliferative (active) STICs; yellow bars, dormant STICs; green bars, p53 signatures.

IGV. Among the 1261 confirmed somatic mutations, 267 were synonymous and 994 were non-synonymous mutations (see supplementary material, Table S3). All 18 precursor lesions harbored somatic mutations and there were 39 non-synonymous mutations involving 12 canonical cancer-driver genes (see supplementary material, Table S3) [24]. Among these 12 cancer-driver genes, only *TP53* was mutated in more than one patient; the finding is similar to previous studies [16,21,27,28]. All tubal lesions in this study cohort including p53 signature and 'dormant STIC' (STIL) harbored somatic mutation in *TP53* (Table 1). The average number of somatic mutations identified in p53 signatures was lower than the numbers identified in dormant STIC; however, the data did not reach statistical significance (Figure 2B). Notably, incidental STICs without concurrent HGSC harbored fewer somatic mutations than those co-existing with HGSC (see supplementary material, Figure S2A; $p = 0.0121$, Mann–Whitney test).

Whole-exome data for all lesions were also analyzed for genome-wide allelic imbalance and regional LOH events (see supplementary material, Table S4 and Figure 2A). As expected, LOH events per lesion were most frequently detected in ovarian HGSC (median 17.5), followed by STICs (median 7) and rarely in dormant STICs or p53 signatures (median 0, Kruskal–Wallis test, $p = 0.011$). However, pairwise comparisons among p53 signature, dormant STIC and STIC did not reach statistical significance (Figure 2C). On the other hand, the number of LOH events between STICs with or without concurrent HGSC differed significantly (median 18 versus 3.5, $p = 0.0364$; Mann–Whitney test) (see supplementary material, Figure S2B). LOH spanning the entirety of chromosome 17, which contains *TP53* and *BRCA1*, was identified in 10 of 18 (56%) tubal precursor lesions (Table 1). In addition, five of 18 (28%) tubal precursor lesions exhibited LOH of the entire chromosome 13, which contains *BRCA2* and *RB1* (Table 1). Integrated profiles of somatic mutation and LOH events for each patient were generated (see supplementary material, Figure S3). If we consider both somatic mutations and LOH events as molecular genetic alterations, there was an increase of such alterations in HGSCs compared with other precursor lesions (Figure 2D) and the combined events in p53 signatures was significantly less than that in HGSCs ($p = 0.0138$; Kruskal–Wallis test with Dunn's *post-hoc* test), but not for other pairwise comparisons. STICs without associated ovarian HGSC had fewer alterations than STICs with associated ovarian HGSC (median 37 versus 105, $p = 0.0121$; Mann–Whitney test; see supplementary material, Figure S2C). It remains possible that STIC lesions

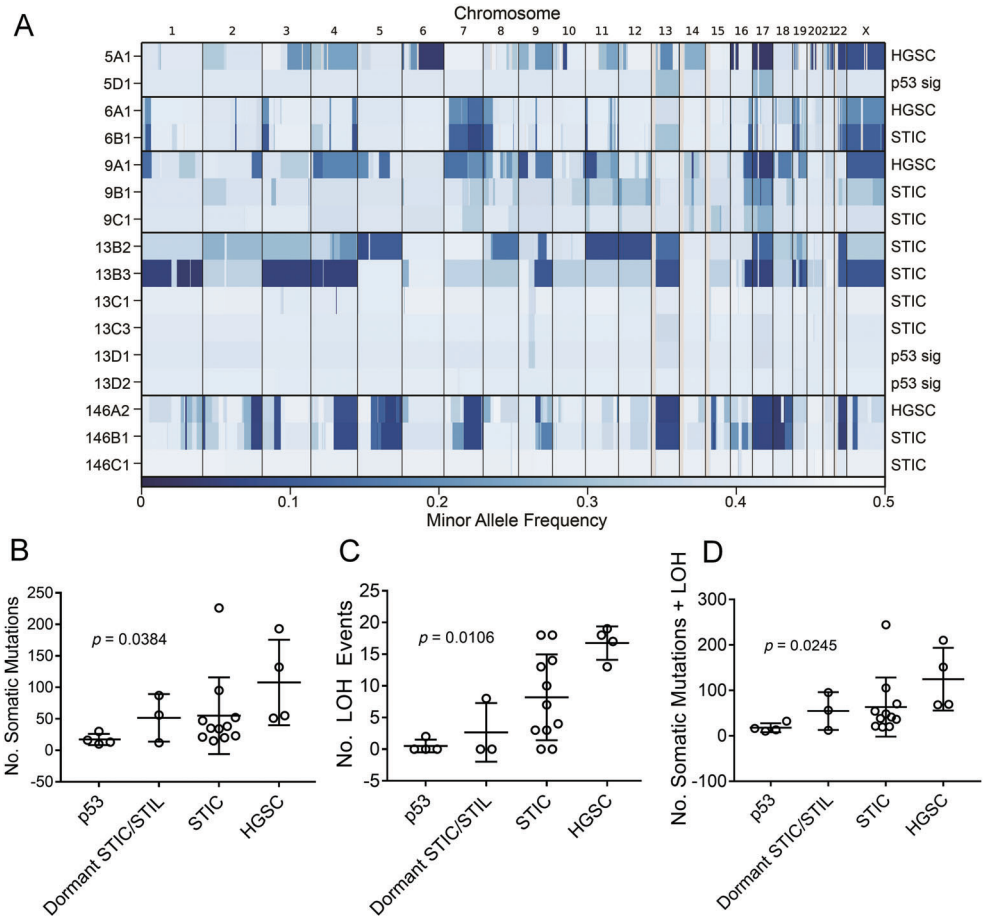

Figure 2. Genome-wide allelic imbalance analysis. (A) Genome-wide allelic imbalance profiles. Minor allele frequencies of heterozygous SNPs identified from normal samples were calculated for each lesion sample and segmented using the circular binary segmentation algorithm. The mean minor allele frequencies of chromosomal segments are depicted as a heatmap. In cases 6, 9 and 146, different lesions from the same individual shared segments of allelic imbalance, suggesting clonal relationships between these lesions. In contrast, there are no shared subchromosomal segments of allelic imbalance among different lesions in cases 5 and 13. (B–D) Comparison in the numbers of genetic alterations per lesion among different precursors and HGSC. Data are presented as mean ± SD. *P* values were calculated using the Kruskal–Wallis test.

with co-existing ovarian HGSC represent disseminated clones from ovarian HGSC, which may morphologically mimic bona fide STICs. Therefore, the difference of mutation loads between STICs with concurrent ovarian HGSC versus incidental STICs should be interpreted with caution.

Based on genetic alterations including somatic mutations and LOH, we performed phylogenetic analysis, which provided a means of inferring the history of tumor clonal evolution in patients harboring multiple lesions (cases 5, 6, 9, 13 and 146). Case 13 was a patient without a diagnosis of cancer who had six discrete tubal lesions in her bilateral Fallopian tubes including three p53 signatures, one dormant STIC and two STICs (Figure 3A). Each of the lesions harbored a non-identical *TP53* mutation and other private mutations with the exception being two lesions, 13C3 and 13D2, which shared three mutations including *BRD4* (Table 1 and Figure 3B). Therefore, the lesions found in this woman, including 13C1, 13D1, 13B2, 13B3 and 13C3/D2, probably originated from independent cellular events and evolved in parallel (Figure 3B).

The STIC lesions in three (cases 6, 9, 146) of the four (cases 5, 6, 9, 146) patients with co-existing ovarian HGSCs were clonally related to their corresponding ovarian carcinoma, as their precursor lesions shared identical *TP53* mutations and other truncal mutations with their ovarian carcinoma counterpart (Table 1 and Figure 4). The p53 signature in the other patient (case 5) did not share any somatic mutations or subchromosomal LOH with the corresponding ovarian carcinoma. Therefore, the p53 signature of case 5 was considered not clonally related to ovarian HGSC from this patient (Figure 4).

We further applied amplicon sequencing to analyze *TP53* mutations in four women (cases 12, 15, 16 and 111) with incidental precursor lesions that were too small to perform whole-exome sequencing. In cases 12, 15 and 111, in whom multiple precursor lesions were present, non-identical *TP53* somatic mutations were found in each of the lesions from the same patient (Table 1). These findings, together with findings from cases 5 and 13, provide compelling evidence that at the very early stage of tubal tumorigenesis, precursor

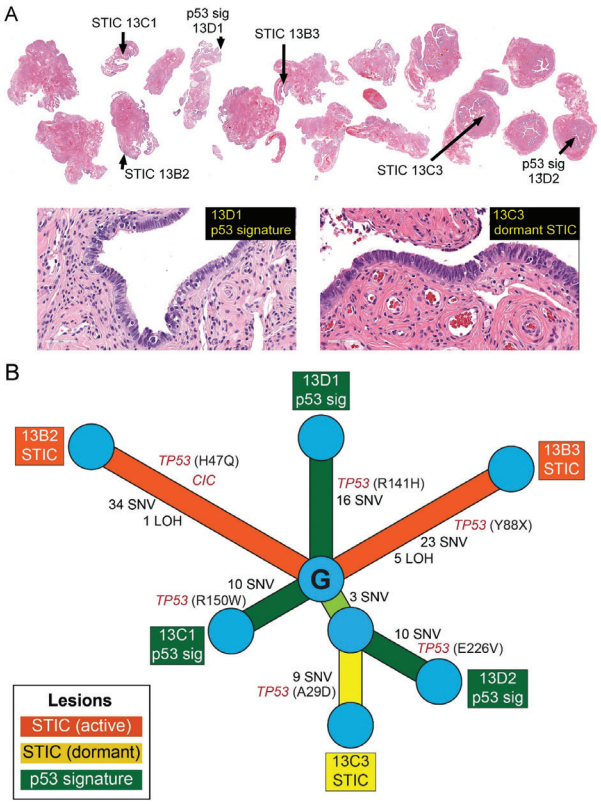

Figure 3. Genomic analysis of incidental tubal lesions in case 13 without concurrent or a history of cancer. (A) Top: the locations of six distinct lesions on Fallopian tube tissue sections. Bottom: representative photomicrographs of two lesions and their corresponding *TP53* mutation status. (B) The phylogenetic tree of multiple lesions in case 13.

lesions may arise from independent cellular origins and probably co-exist for many years before one (or very few) clone undergoes clonal expansion.

Next, we estimated the time required for a precursor lesion to develop into a full-blown HGSC. We modeled the numbers of mutations that accumulated by time (t) in the cell lineage of the Fallopian tube epithelium as an inhomogeneous Poisson process, with its λ parameter depending on the specific stage of the lesion. Ki-67 labeling indicated no significant difference in proliferation rates between cells in normal epithelium and cells in p53 signature lesions (see Table 1 and reference [20]). We therefore used the number of mutations found in each of the three available p53 signature lesions to estimate the λ parameter of the Poisson process in normal epithelium via MLE and calculated that $\lambda = 0.39$ (details are described in Materials and methods). Based on this number, we estimated that in normal Fallopian tube epithelium, the whole exome of each cell accumulates 0.39 mutations per year. It has been shown that proliferatively active STIC lesions and ovarian HGSC generally have similar Ki-67-positive labeling indices, which are 17-fold greater than the indices found in normal tubal epithelium [29]. This yields an average of 6.5 accumulated mutations per whole exome per cell per year in ovarian HGSC and in STIC. To increase the precision of our estimate, we used a lesion-specific Ki-67-positive labeling index (proliferation rate) to derive the λ parameter for each lesion and built a tumor evolution phylogenetic timeline (see supplementary material, Figure S4 and Table 1). Using this approach, we found that p53 signature lesions appeared to arise relatively early in a woman's life, ranging between 35 and 45 years at the latest (Table 1). Case 146 has concurrent dormant and active STICs in addition to ovarian HGSC, so it served as an index model to estimate the evolutionary time from precursor lesions to ovarian HGSC. Using the lesion-specific proliferation rate as mentioned above, this patient was estimated to have acquired the *TP53* mutation by age 35 years and it took a prolonged time (34 years) to develop into an active STIC. However, the progression from active STIC to ovarian HGSC was relatively fast (~6 years) (see supplementary material, Figure S4 and Table 1).

A potential limitation of this approach is that the proportion of proliferating epithelial cells – and therefore the percentage of Ki-67-labeled epithelial cells – may not be constant, even along a single edge of the phylogenetic evolution tree. However, the over- or under-estimation will be much smaller than would be the case if a single constant proliferation rate is used for all edges of the lesions, disregarding fitness advantages, as typically performed in standard approaches [30].

Discussion

To the best of our knowledge, this is the largest study performing whole-exome mutational landscape analysis on p53 signatures, dormant STICs and proliferative STICs from cancer-free women, although a recent study has also analyzed a few such lesions [27]. We found that, compared with tubal lesions associated with ovarian cancer, these incidental tubal lesions have fewer somatic mutations or allelic imbalances, indicative of their earlier occurrence in the tumor evolution timeline. Additionally, incidental precursor lesions from the same individual can be initiated at different time points and from different cellular origins rather than simultaneously; many of them did not harbor identical *TP53* mutations or share truncal mutations. The data collected from the very early stages of tubal lesions provide new insights indicating that tumor evolution does not necessarily follow a linear evolutionary track at the beginning [21].

Multiclonal tubal precursor lesions have been seen in a small fraction of patients in our previous study, in which we applied *TP53* target-based sequencing on 29 patients with concurrent ovarian or pelvic HGSC and multiple STIC lesions. In this cohort, although most STICs and ovarian HGSC from the same patient were clonally related, at least four patients harbored non-identical *TP53* mutations in their multiple STIC lesions, indicating clonal independence between these lesions (table 1 in reference [19]). Indeed, based on the observation of clonal heterogeneity in ovarian cancers,

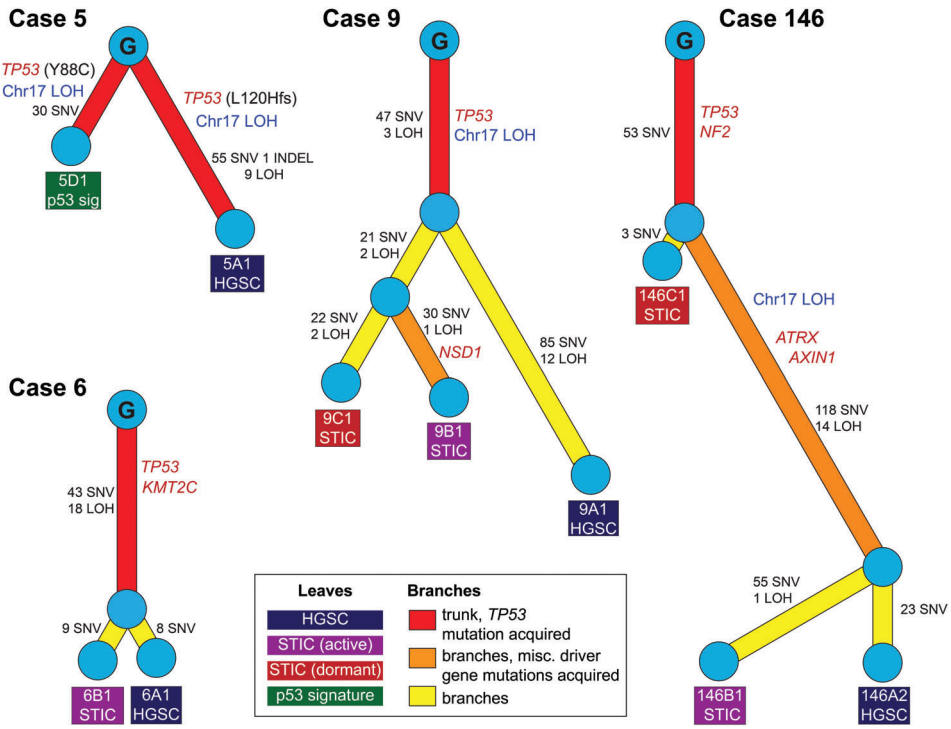

Figure 4. Phylogenetic trees of cases with concurrent tubal precursors and ovarian HGSC. Branch length was proportional to the number of somatic mutations and subchromosomal LOH; longer branches indicate more genomic differences. Evolutionary branching patterns reflect clonal relationships between lesions. Branches are labeled with cancer-driver genes as well as numbers of accumulated mutations and LOH events. Circles marked with 'G' indicate the ancestral (germline) clone.

polyphyletic clonal development track at the early stage of tumor evolution has also been implicated previously by Bashashati *et al* [21]. Through analysis of the earliest precursor lesions, the current study provides some of the first experimental data supporting this concept. Phylogenetic analysis on patients with concurrent precursor lesions and ovarian HGSC showed that some tubal lesions were probably not the immediate precursors of ovarian cancer, further supporting the above view. For example, lesion 5D1 in case 5 and lesions 9B1 and 9D1 in case 9 harbor numerous private mutations distinguishing them from the corresponding ovarian cancer; therefore, even though they co-exist with the ovarian cancer, these lesions either arose from a different event (such as 5D1) or diverged very early in the evolutionary timeline (such as 9B1 and 9D1) (Figure 4).

Our findings indicate that the rate of cell replication is distinct in different stages during tumor evolution. The Ki-67 proliferation index in p53 signature and in dormant STIC was low and often indistinguishable from the adjacent normal tubal epithelium. On the other hand, proliferative STICs and ovarian HGSCs displayed increased cellular proliferation. This distinction provides a molecular basis for our multisegment tumor evolutionary timeline calculation, which is based on the number of genetic alteration events and on tissue and lesion-specific proliferation rates. On the other hand, phylogenetic tree analysis does not take the latter factor into consideration. According to the estimate, the majority of precursor lesions developed when women were in their late teens or early twenties, suggesting a prolonged latency from the acquisition of *TP53* mutation to progression. Therefore, it may take at least two decades from the appearance of a p53 signature lesion to the development of ovarian cancer. This relatively broad window of progression may, in principle, allow sufficient time for early detection of precancerous lesions for future intervention. However, it takes only about 6 years for proliferative STICs to progress into ovarian HGSC, indicating accelerated tumor progression during this stage, and a much shorter window for effective intervention [31].

There are conceivable limitations of this study. First, although we detected a trend of increased number of genetic alterations from p53 signature to STICs, statistical significance was not reached. It is likely that a large multi-institutional consortium will be needed to validate the findings. Second, the minute precursor lesions imposed a technical challenge for acquiring specimens with high tumor purity, especially for p53 signatures. Furthermore, the sequencing coverage in whole-exome data may not be high enough to accurately infer DNA copy number alteration or to build subclonal structures. Consequently, phylogenetic relationships established in this study did not take subclonal structures into consideration. On the other hand, in most of the precursor lesions (except for cases 11B1, 13D2 and 145B1), we observed that *TP53* mutant allele frequency was among the highest and was approximately two-fold greater than the median mutant allele frequency of other gene mutations identified in the same lesions. Therefore, *TP53* mutation was probably clonal in the majority of lesions. The data

also imply that clonal expansion accompanied by allelic imbalance at the *TP53* locus occurred very early in precursor lesion development.

To elucidate the biological and molecular characteristics of tubal lesions in the precancer stage, we used 'dormant' to describe atypical tubal precursor lesions with low proliferation rates (Ki-67 index <10%). Although 'dormant STIC' and p53 signature lesions harbor somatic mutations in *TP53* and, sometimes, mutations in several other cancer-driver genes, they remain 'dormant' and clinically 'occult' for a prolonged period of time. The reason that these lesions stay in an inert, non-proliferative state is elusive. Potential mechanisms include, but are not limited to, telomere shortening, oncogene-induced cellular senescence and effective immune function in healthy individuals [3]. For the latter possibility it will be important to delineate factors in the host immune microenvironment that keep these mutated and clonally expanded precursor lesions in check [32]. Equally important will be to identify biomarkers capable of distinguishing benign or dormant precursor lesions from those that may progress. The findings presented here may shed light on future research directions in prevention and early detection, keys to reducing the incidence and mortality of ovarian cancer.

Acknowledgements

The authors appreciate the technical assistance of Ms Asli Bahadirli-Talbott and Ms Zoe Wang, and critical comments from Dr Herman Chui. This work was supported by the US Department of Defense CDMRP (grant number W81XWH-11-2-0230); the National Key Basic Research Program of China (973 program) (grant number 2015CB553902), the National Institutes of Health/National Cancer Institute (grant numbers UO1CA200469, RO1CA215483, P50CA228991, P30CA006973); the Honorable Tina Brozman Foundation, Ovarian Cancer Research Fund Alliance, Roseman Foundation; Teal Award, and Gray Foundation; the John Templeton Foundation; the Gynecologic Pathology Laboratory of Richard W. TeLinde Endowment, Johns Hopkins University; the National Natural Science Foundation Fund of China (grant number 81472559); Peking Union Medical College Fundamental Research Funds (grant numbers JK2013A21, JK2014B10); the CAMS Innovation Fund for Medical Sciences (CIFMS) (grant numbers 2016-I2M-1-001).

Author contributions statement

SFL, PW, RCW, YJ, TLW and IMS conceived and designed the study. RJK, RV, IMS and BGW reviewed cases. SFL, PW, MZ, KK, YJ and RCW performed experiments. RCW, SFL, TC and CT performed the statistical analysis. CT performed the mathematical modeling. RCW and QS performed the bioinformatics analysis. RCW, SFL, CT, IMS and TLW wrote the manuscript.

References

1. Trabert B, Coburn SB, Mariani A, *et al.* Reported incidence and survival of Fallopian tube carcinomas: a population-based analysis from the North American Association of Central Cancer Registries. *J Natl Cancer Inst* 2017; **110:** 750–757.
2. Skates SJ, Greene MH, Buys SS, *et al.* Early detection of ovarian cancer using the risk of ovarian cancer algorithm with frequent CA125 testing in women at increased familial risk – combined results from two screening trials. *Clin Cancer Res* 2017; **23:** 3628–3637.
3. Kuhn E, Meeker A, Wang T-L, *et al.* Shortened telomeres in serous tubal intraepithelial carcinoma: an early event in ovarian high-grade serous carcinogenesis. *Am J Surg Pathol* 2010; **34:** 829–836.
4. Kuhn E, Wang T-L, Doberstein K, *et al.* CCNE1 amplification and centrosome number abnormality in serous tubal intraepithelial carcinoma: further evidence supporting its role as a precursor of ovarian high-grade serous carcinoma. *Mod Pathol* 2016; **29:** 1254–1261.
5. Kuhn E, Kurman RJ, Shih I-M. Ovarian cancer is an imported disease: fact or fiction? *Curr Obstet Gynecol Rep* 2012; **1:** 1–9.
6. Visvanathan K, Wang T-L, Shih I-M. Precancerous lesions of ovarian cancer – a US perspective. *J Natl Cancer Inst* 2017; **110:** 692–693.
7. Ducie J, Dao F, Considine M, *et al.* Molecular analysis of high-grade serous ovarian carcinoma with and without associated serous tubal intra-epithelial carcinoma. *Nat Commun* 2017; **8:** 990.
8. Lee Y, Miron A, Drapkin R, *et al.* A candidate precursor to serous carcinoma that originates in the distal fallopian tube. *J Pathol* 2007; **211:** 26–35.
9. Piek JM, van Diest PJ, Zweemer RP, *et al.* Dysplastic changes in prophylactically removed fallopian tubes of women predisposed to developing ovarian cancer. *J Pathol* 2001; **195:** 451–456.
10. Medeiros F, Muto MG, Lee Y, *et al.* The tubal fimbria is a preferred site for early adenocarcinoma in women with familial ovarian cancer syndrome. *Am J Surg Pathol* 2006; **30:** 230–236.
11. Kindelberger DW, Lee Y, Miron A, *et al.* Intraepithelial carcinoma of the fimbria and pelvic serous carcinoma: evidence for a causal relationship. *Am J Surg Pathol* 2007; **31:** 161–169.
12. Visvanathan K, Shaw P, May BJ, *et al.* Fallopian tube lesions in women at high risk for ovarian cancer: a multicenter study. *Cancer Prev Res* 2018; **11:** 697–706.
13. Vang R, Visvanathan K, Gross A, *et al.* Validation of an algorithm for the diagnosis of serous tubal intraepithelial carcinoma. *Int J Gynecol Pathol* 2012; **31:** 243–253.
14. Visvanathan K, Vang R, Shaw PA, *et al.* Diagnosis of serous tubal intraepithelial carcinoma based on morphologic and immunohistochemical features: a reproducibility study. *Am J Surg Pathol* 2011; **35:** 1766–1775.
15. Rabban JT, Vohra P, Zaloudek CJ. Nongynecologic metastases to fallopian tube mucosa: a potential mimic of tubal high-grade serous carcinoma and benign tubal mucinous metaplasia or nonmucinous hyperplasia. *Am J Surg Pathol* 2015; **39:** 35–51.
16. Eckert MA, Pan S, Hernandez KM, *et al.* Genomics of ovarian cancer progression reveals diverse metastatic trajectories including intraepithelial metastasis to the Fallopian tube. *Cancer Discov* 2016; **6:** 1342–1351.
17. McDaniel AS, Stall JN, Hovelson DH, *et al.* Next-generation sequencing of tubal intraepithelial carcinomas. *JAMA Oncol* 2015; **1:** 1128–1132.

18. Singh R, Cho KR. Serous tubal intraepithelial carcinoma or not? Metastases to Fallopian tube mucosa can masquerade as in situ lesions. *Arch Pathol Lab Med* 2017; **141:** 1313–1315.
19. Kuhn E, Kurman RJ, Vang R, *et al.* TP53 mutations in serous tubal intraepithelial carcinoma and concurrent pelvic high-grade serous carcinoma – evidence supporting the clonal relationship of the two lesions. *J Pathol* 2012; **226:** 421–426.
20. Alves JM, Prieto T, Posada D. Multiregional tumor trees are not phylogenies. *Trends Cancer* 2017; **3:** 546–550.
21. Bashashati A, Ha G, Tone A, *et al.* Distinct evolutionary trajectories of primary high-grade serous ovarian cancers revealed through spatial mutational profiling. *J Pathol* 2013; **231:** 21–34.
22. Yemelyanova A, Vang R, Kshirsagar M, *et al.* Immunohistochemical staining patterns of p53 can serve as a surrogate marker for TP53 mutations in ovarian carcinoma: an immunohistochemical and nucleotide sequencing analysis. *Mod Pathol* 2011; **24:** 1248–1253.
23. Wang K, Li M, Hakonarson H. ANNOVAR: functional annotation of genetic variants from high-throughput sequencing data. *Nucleic Acids Res* 2010; **38:** e164.
24. Tokheim CJ, Papadopoulos N, Kinzler KW, *et al.* Evaluating the evaluation of cancer driver genes. *Proc Natl Acad Sci U S A* 2016; **113:** 14330–14335.
25. Felsenstein J. PHYLIP - phylogeny inference package (version 3.2). *Cladistics* 1989; **5:** 164–166.
26. Merritt MA, De Pari M, Vitonis AF, *et al.* Reproductive characteristics in relation to ovarian cancer risk by histologic pathways. *Hum Reprod* 2013; **28:** 1406–1417.
27. Labidi-Galy SI, Papp E, Hallberg D, *et al.* High grade serous ovarian carcinomas originate in the fallopian tube. *Nat Commun* 2017; **8:** 1093.
28. McPherson A, Roth A, Laks E, *et al.* Divergent modes of clonal spread and intraperitoneal mixing in high-grade serous ovarian cancer. *Nat Genet* 2016; **48:** 758–767.
29. Kuhn E, Kurman RJ, Sehdev AS, *et al.* Ki-67 labeling index as an adjunct in the diagnosis of serous tubal intraepithelial carcinoma. *Int J Gynecol Pathol* 2012; **31:** 416–422.
30. Jones S, Chen WD, Parmigiani G, *et al.* Comparative lesion sequencing provides insights into tumor evolution. *Proc Natl Acad Sci U S A* 2008; **105:** 4283–4288.
31. Song M, Vogelstein B, Giovannucci EL, *et al.* Cancer prevention: molecular and epidemiologic consensus. *Science* 2018; **361:** 1317–1318.
32. Albrengues J, Shields MA, Ng D, *et al.* Neutrophil extracellular traps produced during inflammation awaken dormant cancer cells in mice. *Science* 2018; **361:** pii: eaao4227.

SUPPLEMENTARY MATERIAL ONLINE

Supplementary materials and methods

Figure S1. Representative images of precancerous lesions in the Fallopian tube

Figure S2. Comparison of somatic mutations and LOH events identified in STICs from women with or without ovarian HGSC

Figure S3. Integrated profiles of somatic mutation and LOH events for lesions in all patients

Figure S4. Evolutionary timeline inferred based on proliferation rate and genetic alteration events

Table S1. Clinical information for each patient

Table S2. Sequence analysis summary of whole exome sequencing on 46 specimens

Table S3. Full list of somatic mutations identified in each lesion

Table S4. Full list of LOH events identified in each lesion